Published online 24 May 2011

Nucleic Acids Research, 2011, Vol. 39, No. 15 ***e99***
doi:10.1093/nar/gkr293

Hybridization kinetics between immobilized double-stranded DNA probes and targets containing embedded recognition segments

Bryan A. Baker[1] and Valeria T. Milam[1,2,3,*]

[1]School of Materials Science and Engineering, [2]Wallace H. Coulter Department of Biomedical Engineering and [3]Petit Institute for Bioengineering and Bioscience, Georgia Institute of Technology, 771 Ferst Dr. NW, Atlanta, GA 30332-0245, USA

Received September 19, 2010; Revised April 5, 2011; Accepted April 14, 2011

ABSTRACT

We have investigated the time-dependent strand displacement activity of several targets with double-stranded DNA probes (dsProbes) of varying affinity. Here, the relative affinity of various dsProbes is altered through choices in hybridization length (11–15 bases) and the selective inclusion of center mismatches in the duplexes. While the dsProbes are immobilized on microspheres, the soluble, 15 base-long complementary sequence is presented either alone as a short target strand or as a recognition segment embedded within a longer target strand. Compared to the short target, strand displacement activity of the longer targets is slower, but still successful. Additionally, the longer targets exhibit modest differences in the observed displacement rates, depending on the location of recognition segment within the long target. Overall, our study demonstrates that the kinetics of strand displacement activity can be tuned through dsProbe sequence design parameters and is only modestly affected by the location of the complementary segment within a longer target strand.

INTRODUCTION

A hallmark of DNA is the complementary base pairing that naturally occurs between two single oligonucleotide strands to form a double-stranded helical segment or duplex (1). These initial duplex formation or primary hybridization events have been widely studied between soluble target strands and single-stranded DNA (ssDNA) immobilized on a planar substrate (2–8) or, to a much lesser extent, on colloidal particles (9–12). For these studies, monitoring the conversion of ssDNA into duplexes is reported using some intrinsic or secondary labeling step, often fluorescence based. While hybridization of perfectly complementary targets to their respective probe strands is expected to occur preferentially, targets containing mismatches can also successfully hybridize to probe strands. Since a specific target sequence is often sought for capture through hybridization events, a key issue involves either minimizing hybridization activity between mismatched partner strands or differentiating the hybridization behavior of mismatched targets from that of perfectly matched targets. One reported approach to promote hybridization of perfectly matched targets over that of mismatched targets involves incubating oligonucleotides under elevated temperature conditions (13), while other methods involve the intentional inclusion of known mismatched immobilized strands or probe sequences to establish a baseline for non-specific probe–target associations (2,14,15). These approaches, however, may be less effective at screening out targets possessing mismatched bases near the ends of the target strand (16,17) than targets possessing mismatches near or at the duplex center. As opposed to relying exclusively on the end points following assay completion, other studies suggest that a measure of target specificity can be deduced by analyzing the kinetics of primary hybridization events between single-stranded oligonucleotide probes and targets (18–23).

Historically, hybridization studies have focused on primary duplex formation, however, the related, but distinct process of strand displacement has more recently garnered attention. In a strand displacement event, the target strand must replace the original partner strand of the initial or primary duplex to form a new or secondary duplex. This exchange of partner strands can be reported by either a signal-on event (e.g. a quenched fluorophore becomes fluorescent following duplex formation with a target) or a signal-off event (e.g. the initial duplex

*To whom correspondence should be addressed. Tel: +1 404 894 2845; Fax: +1 404 385 3734; Email: valeria.milam@mse.gatech.edu

contains a fluorescently labeled strand that is removed as a secondary duplex forms). Successful displacement is promoted if the target of interest has a greater affinity for one of the strands in the initial duplex or double-stranded probe (dsProbe). Thus, in terms of effective reporting, the ideal dsProbes possess (i) sufficient base-pair matches to remain thermally stable in the absence of a target of interest, but (ii) fewer base-pair matches than the target of interest. Early experimental efforts used chromatography to monitor the displacement of a shorter DNA strand (1.6 Kb) by a much longer strand (6.1 Kb) in oligonucleotide solutions (24). In other early studies, the duplex region of the probe was comprised of an RNA–DNA hybrid in which the displaced RNA was detected through a multistep bioluminescence approach (25,26). Related experimental efforts incorporated intentional single base-pair mismatches within the duplex region of the dsProbes (27). While target detection serves as an important motivation for many hybridization studies involving dsProbes (28–34), these strand displacement events play a pivotal role in other scenarios such as DNA-based devices and machines in which oligonucleotides serve as a fuel strand (35–39), isothermal redispersion of DNA-linked particles (40–43) and even reconfiguration of gold nanoparticle spacing in an assembly structure (44,45). In each of these systems highlighted above, a single-stranded region is typically included in the primary duplex to act as a toehold or nucleation site for the target to initiate hybridization. While long, single-stranded toehold regions were characteristic of many early studies, as few as three bases are needed to establish a stable duplex nuclei and facilitate the branch migration that precedes displacement of the original hybridization partner (46). While strand displacement-based approaches continue to gain popularity in the rational design of many systems, the discussion of strand displacement kinetics is less prevalent and focuses almost exclusively on oligonucleotide solutions in which both the dsProbes and targets are soluble species (24,25,27,29,47). Recent reports by Zhang and Winfree (48) and Genot *et al.* (49), for example, have particularly focused on the kinetics of these displacement events for driving DNA-based reaction schemes in oligonucleotide solutions. Even fewer kinetics studies address immobilized double-stranded DNA probe (dsProbe) systems (26,28). Collectively, however, these reports demonstrate the versatility of these systems for characterizing hybridization behavior, especially if colloidal substrates (28,42) are employed such as the microspheres used in the current kinetics study.

While target capture and signaling steps often occur separately (9,13,50), our approach links these two events into one step to enable a straightforward analytical approach monitoring fluorescence loss due to the time-dependent release of fluorescently tagged reporter strands from the original duplexes or dsProbes. This report specifically considers the role that sequence design of the dsProbe plays on the kinetics of strand displacement for multiple related, but distinct targets in which the hybridization segment is identical, but spatially located at different segments in the target strand. The relative affinity of the dsProbes is tuned through variations in duplex length as well as the selective inclusion of a center base-pair mismatch. Here, we use flow cytometry to quantify changes in the density of fluorescently tagged dsProbes immobilized on polystyrene microspheres. The following study compares several dsProbe systems to detect two categories of targets: (i) a short 15 base-long DNA target corresponding to the *rrl* sequence of the *Salmonella* genome (9) and (ii) the same 15 base-long recognition segment embedded in longer targets with non-complementary or nonsense segment(s) comprised of 85 thymine bases. For these long targets, the 15 base-long recognition sequence is incorporated at different locations within the DNA strand. Similar to molecular beacons that function by identifying a recognition sequence within a long mRNA strand context (51), the current work aims to further elucidate the effects of target strand context in strand displacement events. Recent studies by Plaxco and coworkers (52) indicate similar hybridization kinetics occur for long targets with stem-loop probes, independent of the orientation of any unhybridized bases remaining near the 3′- or 5′-end of the target. For single-stranded linear probes, however, the orientation of this unhybridized tail had a more pronounced effect on hybridization kinetics (52). The current study complements this prior work on single-stranded probes by comparing the kinetics of hybridization between dsProbes and various long targets possessing embedded complementary segments. The results of this study contribute to further understanding of strand displacement events, particularly those occurring on immobilized supports. Additionally, the effect of sequence design on dsProbe affinity and its impact on strand displacement is considered. The important consideration, for example, of mismatch discrimination by strand displacement approaches will be addressed in separate work.

MATERIALS AND METHODS

Materials

DNA strands were purchased HPLC-purified from Integrated DNA Technologies (IDT, Coralville, IA, USA). An amine group attached to the 5′-end of sequences (to be immobilized) was separated from the 15 DNA bases by a 12 carbon spacer. Soluble 11, 13 or 15 base-long reporter strands comprised of either perfectly complementary or center mismatched sequences were fluorescein-labeled at the 5′-end. The nomenclature used to describe these sequences is illustrated by the example of **T11**, an 11 base-long sequence that is perfectly complementary to the 15 base-long immobilized **P15** strand. The resulting dsProbe is listed as **P15:T11**. All target candidates possess a 15 base-long segment that is perfectly complementary to the immobilized **P15** sequence. The short 15 base-long perfectly complementary target (**T15**) as well as all 100 base-long targets are unlabeled. After purchase, DNA sequences were stored as 100 μM aliquots at −20°C in Tris/EDTA (TE) buffer. Fluorescein-labeled sequences (incorporated via a modified thymine not

intended for any hybridization events) were stored in TE pH 8.0 and unlabeled sequences in TE pH 7.4. The 5.1 μm carboxylate-modified latexes (CML) were purchased from Molecular Probes (Molecular Probes, Eugene, OR, USA). *N*-Ethyl-*N*′-(3-dimethylaminopropyl) carbodiimide hydrochloride (EDAC) was purchased from Sigma (St. Louis, MO, USA). PBS/Tween and coupling buffers were prepared using DIamond Nanopure water (Barnstead International). PBS/Tween buffer was prepared by mixing 5 ml of 10 × PBS concentrate (Sigma), 45 ml of of nanopure H_2O and 100 μl of Tween 20 (Calbiochem, Gibbstown, NJ, USA) for 1 h with end-over-end mixing. The solution was then filtered through a 0.2 μm syringe cap filter. The coupling buffer contained 50 mM MES and 0.05% Proclin 300 and was adjusted to a pH ~5.2 to mimic the formulation of Bangs Laboratories PolyLink Coupling Kit (Fishers, IN, USA).

Conjugation of ssDNA to microspheres

The ssDNA (**P15**) was immobilized on 5.1 μm particles as detailed previously (41). Briefly, 25 μl of 4% w/v solids CML particles were centrifuged at 9.1 × 1000*g* for 2 min (same for all centrifugation steps) and resuspended in 100 μl of coupling buffer. The particles were again centrifuged and resuspended into 150 μl of coupling buffer. Then, 50 μl of coupling buffer was added to 10 mg of pre-weighed EDAC (stored under nitrogen) and immediately vortexed. A 25 μl volume of EDAC/coupling buffer solution was added to the particle suspension followed by a 200 μl addition of 10 μM of **P15** DNA. After vortexing, the suspension was mixed for 2 h end-over-end. Following mixing, the DNA-coupled particles were centrifuged and washed two times in PBS/Tween buffer and resuspended in 100 μl of PBS/Tween for a final concentration of 1% w/v solids.

Hybridization

To form the dsProbes, 12 μl of the **P15**-coupled particles and 188 μl of PBS/Tween were briefly mixed and centrifuged as detailed above. The supernatant was removed and replaced with 200 μl of PBS/Tween. Then, 200 μl of 10 μM fluorescently labeled reporter strands was added, briefly mixed and incubated for 6 h. The final volume of the suspension was thus 400 μl with a 5 μM concentration of reporter DNA before washing. Three centrifugation steps previously described were performed and particles resuspended with 400 μl of PBS/Tween each time. After final resuspension, 20 μl of the suspension was removed and diluted to a final volume of 100 μl in PBS/Tween and stored at 4–8°C prior to flow cytometry measurements. For competition studies, 20 μl of complementary target DNA at 100 μM was added to the suspension. The final suspension volume was thus again 400 μl with a complementary target concentration of 5 μM before washing. The suspension was mixed end-over-end with aliquots taken from the suspension at specified time points of 0.25, 0.5, 0.75, 1, 6, 24, 48 and 72 h. For each time point, 40 μl of suspension was removed and diluted with 60 μl of PBS/Tween. The sample was centrifuged three times and supernatant replaced with 100 μl of PBS/Tween. Samples were stored at 4–8°C until characterized via flow cytometry.

Flow cytometry

The density of fluorescein-labeled DNA duplexes before and remaining after incubation with unlabeled targets was measured using flow cytometry. Following incubation with targets and washing steps, samples were diluted with 900 μl of PBS/Tween to a total volume of 1 ml. A Becton Dickinson FACS II flow cytometer was used for fluorescence measurements (Becton Dickinson, San Jose, CA, USA). A control sample of unlabeled **P15**-conjugated particles served as a negative control to establish a baseline for microsphere autofluorescence. Calibration curves were generated using FITC fluorescence standards from Bangs Laboratories (Fishers, IN, USA) to convert fluorescence intensity values into the surface density of labeled duplexes. Reported duplex density values represent the average of three separate measurements taken from three separately **P15**-coupled particle suspensions.

Analysis of observed displacement rate, k_{obs}

The kinetics of strand displacement have been reported by Reynaldo *et al.* (47) for oligonucleotide solutions in which the original hybridization partner and the competitive target are identical sequences. This approach has been adapted for the current work with the key difference that we incorporate an affinity difference between the reporter strand and the target strand for the immobilized **P15** sequence. The kinetics of displacement for this system are assumed to be reaction limited as the dsProbes are presented on dispersed particle substrates allowing for facile diffusion of the target strands to the dsProbes. As illustrated in Scheme 1, Reynaldo's analysis considers two possible pathways by which an initial labeled duplex (PT_1^*) could be converted into a secondary duplex (PT_2) when incubated with targets (T_2). Here, the original hybridization partner, T_1^*, is tagged with fluorescein while the competitive target, T_2, is unlabeled. The conversion of PT_1^* into PT_2 can occur by either (i) the dissociation of the PT_1^* duplex followed by the rapid association of T_2 resulting in the formation of PT_2 or (ii) sequential displacement

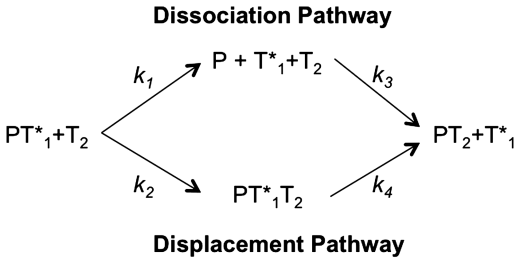

Scheme 1. The two reaction pathways proposed for converting one labeled duplex (PT_1^*) into a secondary unlabeled duplex (PT_2) in the presence of a secondary hybridization partner (T_2) based on analysis by Reynaldo *et al.* (47). In this representation, k_1 is the dissociation rate constant, k_2 is the intermediate complex formation rate constant, k_3 is the association rate constant between T_2 and P and k_4 is the rate constant for converting the intermediate complex $PT_1^*T_2$ into the PT_2 duplex.

of T_1^* from PT_1^* by T_2 involving first the formation of the intermediate complex $PT_1^*T_2$ followed by the rapid displacement of T_1^* and formation of a secondary PT_2 duplex. A critical assumption to Reynaldo's model is that the reverse reaction or reassociation of T_1^* with P does not occur. This assumption does seem reasonable for our system in which both an excess concentration of T_2 as well as sequence-based affinity differences between PT_1^* and PT_2 are likely to favor the formation of PT_2. Also, depending on the preferred pathway, the slowest or limiting reaction rates in Scheme 1 is either k_1 or k_2. Thus, neither k_3 nor k_4 significantly contributes to the observed displacement rate, k_{obs}, further described below.

Given these considerations, the rate of the reaction is expressed in terms of the loss of the species PT_1^*. The fluorescent labeling of T_1^* allows for quantification of duplexes on microspheres using flow cytometry.

$$\frac{d[PT_1^*]}{dt} = -k_1[PT_1^*] - k_2[PT_1^*][T_2] \quad (1)$$

Reynaldo *et al.* (47) combined the contribution of the dissociative and displacement pathways by defining an observed displacement rate, k_{obs}, as follows.

$$k_{obs} = k_1 + k_2[T_2] \quad (2)$$

assuming that $k_3 << k_1$ and $k_4 << k_2$. The solution of this differential equation is the familiar relationship shown below.

$$\frac{[PT_1^*]}{[PT_1^*]_0} = \exp(-k_{obs}t) \quad (3)$$

which describes the fraction of PT_1^* remaining. The fraction of PT_1^* involved in duplex conversion events can, in turn, be described by the following equation:

$$\frac{[PT_1^*]_0 - [PT_1^*]}{[PT_1^*]_0} = 1 - \exp(-k_{obs}t) \quad (4)$$

This expression fits well to an exponential rise to a maximum given by

$$f = f_0 + (f_\infty - f_0)(1 - \exp(-k_{obs} \cdot t)) \quad (5)$$

where f is fraction of reporter strands displaced (or released) at time t, f_0 is fraction displaced (or released) at $t = 0$ which is zero for our system, f_∞ is fraction displaced (or released) at equilibrium, k_{obs} is the observed displacement rate and t is the incubation time with or without targets. As stated previously, Reynaldo *et al.* (47) experimentally determined k_{obs} values for the release of the original hybridization partner within a duplex by an identical sequence and takes into account contributions of both dissociation and displacement. In the current study, we similarly have an excess of T_2, but importantly we also have incorporated a sequence-based affinity difference between PT_1^* and PT_2. Additionally, the data used in our displacement analysis has been normalized to exclude the fraction of PT_1^* lost due to thermal dissociation. By subtracting the fraction of reporter strands released over time from PT_1^* in the absence of targets from the fraction released following incubation with targets, we can determine the contribution of competitive displacement activity to the release profiles to generate displacement profiles. Our reported values for k_{obs} in the current studies are thus attributed exclusively to strand displacement events. The values for k_{obs} were obtained from three-parameter exponential curve fits of time-dependent displacement profiles to Equation (5) using SigmaPlot 11 graphical analysis software. All k_{obs} values reported have an R-squared of 0.9 or higher.

RESULTS

Formation and stability of dsProbes on microspheres

In order to generate dsProbes of varying intrinsic affinity on the **P15**-functionalized microspheres, various hybridization lengths and select mismatches were incorporated in the dye-labeled reporter strands. All hybridization events were quantified using flow cytometry, a popular technique largely implemented in cell studies (53) to quantify receptor–ligand binding events, but adapted here and elsewhere (9,10,54) for particles functionalized with nucleic acids and in high-throughput screening assays of dye-labeled colloids (55). The sequence for each dsProbe system is listed in Table 1 along with our previously reported theoretical duplex melting temperature values (41) based on work by Markham and Zuker (56–58). The resulting initial dsProbe duplex densities on the colloidal particle surface are reported in Figure 1. As expected, trends in the initial duplex density in Figure 1 correspond closely with that of theoretical melting temperatures in Table 1 since higher initial dsProbes densities occur as melting temperature values increase. As the covalent coupling protocol of the immobilized **P15** strand was consistent throughout, any difference in initial density values for the dsProbes is attributed to affinity differences between the 15 base-long immobilized sequence and the various reporter strands. For this study the non-complementary reporter strand (**NC-18**) corresponds to a fluorescently labeled strand comprised of 18 consecutive thymine bases. This sequence was included to test for non-specific interaction between the reporter strand and either the particle surface or immobilized DNA strands. Since fewer than 10 oligos/μm^2 occur for the **NC-18** case, non-specific interactions appear to be negligible in this system. Thus, fluorescence events associated with the remaining complementary or nearly complementary sequences are attributed to hybridization events driving dsProbe formation. For all remaining reporter strands, it was generally observed that dsProbes possessing longer duplex segments result in higher initial dsProbe densities (e.g. 6303 oligos/μm^2 for **P15:T11** versus 12 923 oligos/μm^2 for **P15:T15**). If a center mismatch is included, the duplex density drops significantly for an analogous hybridization segment of equivalent base length. For example, the initial duplex density of a 15 base-long hybridization segment (**P15:T15**) drops from 12 923 oligos/μm^2 to 6392 oligos/μm^2 with the addition of a center mismatch (**P15:T15m**). Based on initial density values, Figure 1 ranks the relative affinity of each

Table 1. List of dsProbe DNA sequences used in flow cytometry studies

dsProbe nomenclature	Sequence	Melting temperature, T_m
P15:NC-18	5′-Amine (12 carbon) CTC GTC ACA CTA TCA-3′ 3′-(Fluor T)TT TTT TTT TTT TTT TTT-5′	NA
P15:T11	5′-Amine (12 carbon) CTC GTC ACA CTA TCA-3′ 3′-AG TGT GAT AGT (T Fluor)-5′	62.4°C
P15:T13	5′-Amine (12 carbon) CTC GTC ACA CTA TCA-3′ 3′-G CAG TGT GAT AGT (T Fluor)-5′	67.8°C
P15:T15	5′-Amine (12 carbon) CTC GTC ACA CTA TCA-3′ 3′-GAG CAG TGT GAT AGT (T Fluor)-5′	71.8°C
P15:T11m	5′-Amine (12 carbon) CTC GTC ACA CTA TCA-3′ 3′-AG TGT CAT AGT (T Fluor)-5′	43.0°C
P15:T13m	5′-Amine (12 carbon) CTC GTC ACA CTA TCA-3′ 3′-G CAG TGA GAT AGT (T Fluor)-5′	58.4°C
P15:T15m	5′-Amine (12 carbon) CTC GTC ACA CTA TCA-3′ 3′-GAG CAG TCT GAT AGT (T Fluor)-5′	59.5°C

The top strand in each duplex is immobilized to a microsphere via the amine terminus. The notation '(T Fluor)' in each reporter strand corresponds to the fluorescein-modified thymine that is not intended to participate in hybridization. Single-stranded bases in dsProbes are highlighted in red and any center mismatches are underlined in the reporter strand. Previously reported theoretical melting temperature values, T_m, for each dsProbe are also shown (41) and were obtained from Zuker (56).

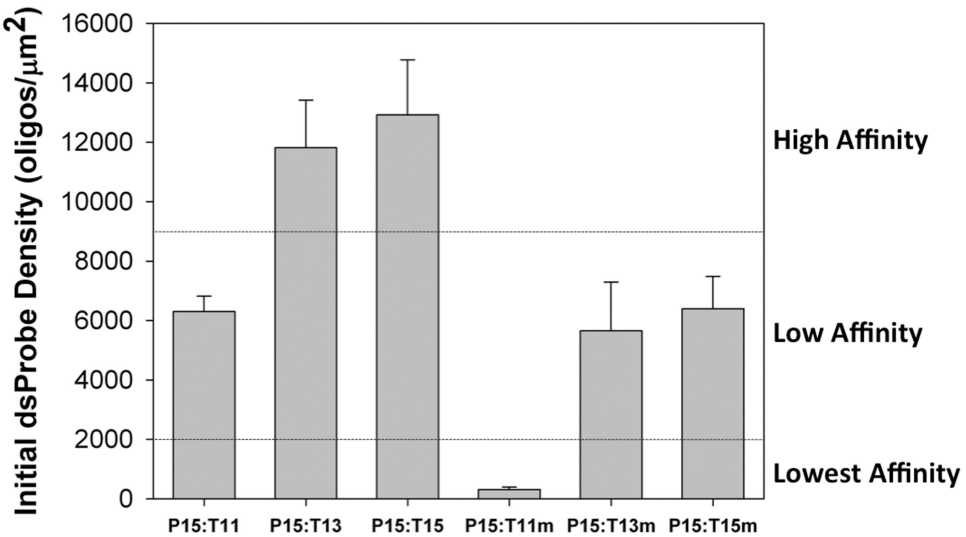

Figure 1. Bar graph of the initial density of the various dsProbes with the relative affinity categories listed to the right.

dsProbe system with the shortest, mismatched **P15:T11m** as the lowest affinity dsProbe and the longest, perfectly matched **P15:T15** as the high affinity dsProbe. Based on the range of duplex density values measured and the particle concentration used, the corresponding dsProbe concentration in the reaction suspension is estimated to be $\sim 10^{-4}$ to 10^{-3} μM. Thus, the 5 μM target concentration used in subsequent strand displacement studies is well in excess of the reporter strand concentration and should favor the forward reaction pathways illustrated in Scheme 1.

After incubating the **P15**-functionalized microspheres with labeled reporter strands to form dsProbes, the suspensions are washed multiple times to remove any unhybridized reporter strands present in the surrounding solution. To test if any reporter strand loss occurs as a result of these washing steps alone, a series of washing studies was performed for **P15:T11**, **P15:T13** and **P15:T15m** dsProbes (Supplementary Figure S1) in the absence of any target strands. These dsProbes were selected as representing both low and high affinity dsProbes as well as complementary and mismatched reporter strand sequences. An aliquot was taken from each of the dsProbe samples after 0, 1, 2, 3, 4, 5 and 6 washing steps, each involving centrifugation and resuspenion. The most noticeable case of fluorescence loss (~17%) as a result of washing steps was observed for the **P15:T11** dsProbe, a low affinity dsProbe, with the greatest loss of reporter strands occurring between wash steps two and four. While this result underscores the need to be aware of the effects of handling on the hybridization process and results, as has been suggested

previously (59), the washing steps themselves only modestly affect the dsProbe density. In the next sections, the time-dependent changes in the density of dsProbes are monitored in the presence of various targets.

Strand release activity of short targets

To begin examining competitive displacement of reporter strands from the dsProbes, an unlabeled perfectly complementary 15 base-long target sequence, **T15**, derived from the *Salmonella* genome (9) was selected as the short target as listed in Table 2. Scheme 2 shows a representative schematic of successful strand displacement events by short targets resulting in the loss of fluorescent reporter strands from the immobilized dsProbes. Figure 2 shows the effects of incubating the various dsProbe systems with the short target over time. With the exception of the high affinity **P15:T15** dsProbe, incubation with **T15** targets results in a significant reduction in the dsProbe density over time, particularly during the first 24 h. Ignoring the lowest affinity dsProbe, **P15:T11m** and the negative control, **P15:NC-18**, the most significant drop in duplex density at early times in Figure 2a occurs for **P15:T11** and **P15:T13m**, two of the low affinity dsProbes. The other low affinity dsProbe, **P15:T15m**, shows a slower though significant loss in duplex density throughout the 72 h experiment as shown in Figure 2b. Notably, both of the low affinity dsProbes exhibiting rapid loss of reporter strands from dsProbes have unhybridized bases next to the original duplex. These adjacent unoccupied bases may serve as a toehold region to facilitate interaction with the **T15** target by acting as a nucleation site for secondary duplexes to form. A similar dependence on duplex length is observed for the two high affinity dsProbes, **P15:T13** and **P15:T15**, in which the **P15:T13** dsProbes containing a toehold exhibit faster and more extensive loss in dsProbe density over the time course of the experiment. The **P15:T15m** dsProbe possesses a center mismatch, but no intentional toehold region is included resulting in successful but slower changes in the dsProbe density. In the absence of any toehold region or mismatch, on the other hand, only a small reduction in duplex density occurs for **P15:T15** dsProbes.

To facilitate more direct comparison between dsProbes with different initial density values as shown in Figure 2, the time-dependent loss of the reporter strand in the presence of **T15** target is presented in Figure 3 as fraction released. Here, the term *release* refers specifically to the loss of the reporter strand from the dsProbe due to both thermal dissociation (in the absence of target) and competitive displacement by the target. The four dsProbe systems shown in Figure 3 represent a low affinity probe with fast release (**P15:T11**), a low affinity dsProbe with moderate release (**P15:T15m**), a high affinity dsProbe with slow release (**P15:T13**) and another high affinity dsProbe with limited release (**P15:T15**). While the initial duplex densities of **P15:T11** and **P15:T15m** are very similar as shown in Table 1, the results shown in Figure 3 more clearly illustrate their differences in release kinetics. Both the **P15:T11** and **P15:T15m** dsProbe systems approach an equilibrium plateau within the time course of the experiment with ~99% and 85% release, respectively. Additionally, the **P15:T11** dsProbe density reaches its plateau value within the first hour while **P15:T15m** density values do not plateau until after 24 h. In contrast to these two low affinity dsProbe cases, the **P15:T13** probe shows continuous displacement throughout the 72 h experiment with 66% total release. The **P15:T15** probe exhibited only 15% release by the 72 h time point and is thus not studied further due to its lack of response to the target studied here. The limited release for **P15:T15** is not surprising since the reporter strand in this dsProbe is the same sequence as the target, thus eliminating sequence-based affinity differences to drive competitive displacement. Overall, the results of

Table 2. List of all target sequences studied

Target nomenclature	Sequence
T15	5′-TGA TAG TGT GAC GAG-3′
NC-100	5′-(T_{100})-3′
3′ End	5′-(T_{85}) TGA TAG TGT GAC GAG-3′
5′ End	5′-TGA TAG TGT GAC GAG (T_{85})-3′
Middle	5′-(T_{42}) TGA TAG TGT GAC GAG (T_{43})-3′

With the exception of the non-complementary 100 base-long sequence, **NC-100,** each target contains the same 15 base-long segment that is complementary to the amine-terminated **P15** sequence shown in Table 1.

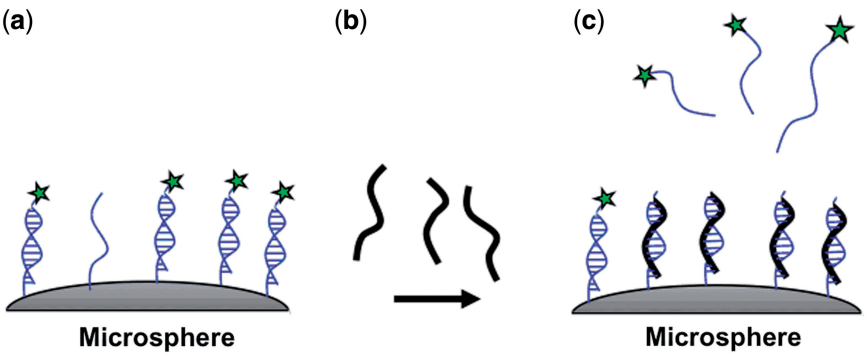

Scheme 2. Illustration of successful strand displacement events in which (**a**) fluorescently labeled dsProbes immobilized on a microsphere substrate are (**b**) incubated with short target strands resulting in (**c**) the displacement of the fluorescently labeled reporter strands from the dsProbes.

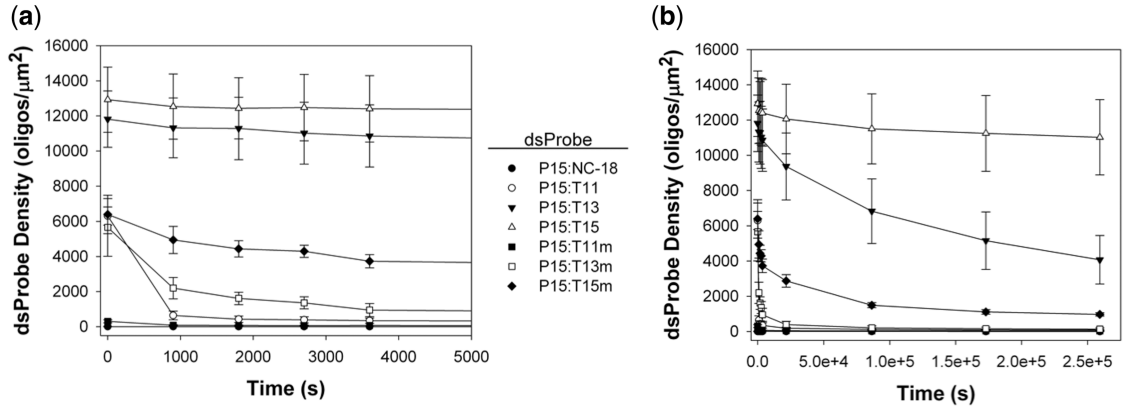

Figure 2. Duplex density of various dsProbes as a function of incubation time with **T15** for the first (**a**)1 h and (**b**) 72 h. Each data point represents the average of three separate measurements with the error bars reflecting the standard deviation about this average.

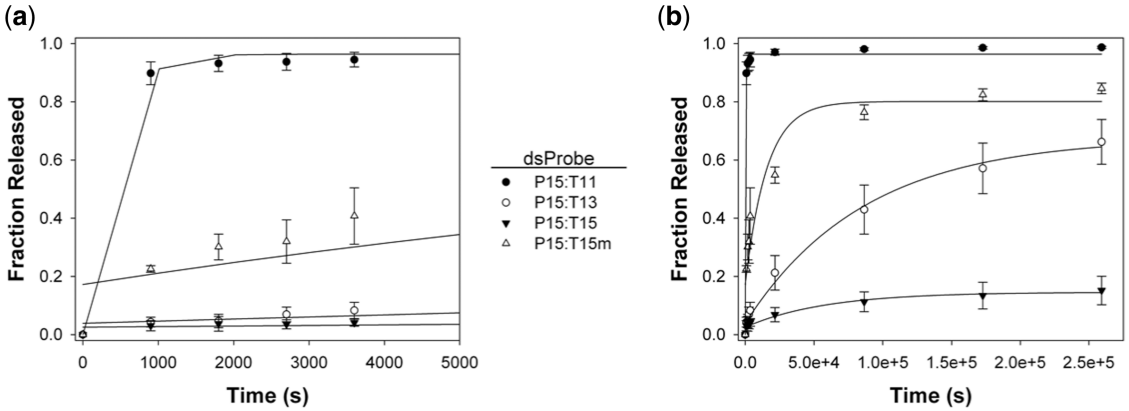

Figure 3. Fraction of reporter strands released from various dsProbes as a function of incubation time with **T15** for the first (**a**) 1 h and (**b**) 72 h. Each data point represents the average of three separate measurements with the error bars reflecting the standard deviation about this average.

these studies with the short 15 base-long competitive target confirm the ability to design dsProbe sequences with distinctive kinetic responses. Three of these dsProbes, **P15:T11**, **P15:T13** and **P15:T15m**, are selected for the next studies with more complicated target systems.

Strand displacement activity of targets with an embedded recognition sequence

We next examine the effects of embedding the **T15** sequence at different locations within a 100 base-long target on strand displacement behavior with three of the dsProbe systems. As shown in Table 2, the 15 base-long complementary segment or recognition sequence was placed at the 3′-end, 5′-end, or in the middle of the long target. A non-complementary 100 thymine only target (**NC-100**) was used to check for non-specific interactions between the dye-labeled targets and either the dsProbes or particle surfaces. As shown in Scheme 3, the likely orientation of the hybridized target relative to the immobilized DNA on the microsphere surface depends on the location of the 15 base-long recognition segment within the target. Based on these structural considerations, the **3′ End** target is expected to be the most effective at displacing the reporter strands as it results in the most advantageous conformation with all unhybridized bases extending away from the microsphere surface as shown in Scheme 3 a. Hybridized **5′ End** targets must bend sharply to allow unhybridized bases to extend into solution away from the microsphere surface. Finally, the **Middle** target has two unhybridized base segments that must be accommodated in order for these secondary duplexes to form. Though not depicted in Scheme 3, some portion of the unhybridized segments may also reside near the microsphere surface, especially for the latter two targets.

Figure 4 shows the release of reporter strands from **P15:T11** dsProbes as a function of incubation time in the absence or presence of various long targets listed in Table 2. To first test dsProbe stability, the immobilized dsProbes were incubated in the same buffer conditions used for hybridization, but in the absence of any complementary targets (this sample is labeled **None**). A second control involved adding the non-complementary target, **NC-100**, to dsProbe-functionalized microspheres. The percentage of reporter strands released for both of these controls (**None** and **NC-100**) were comparable in values,

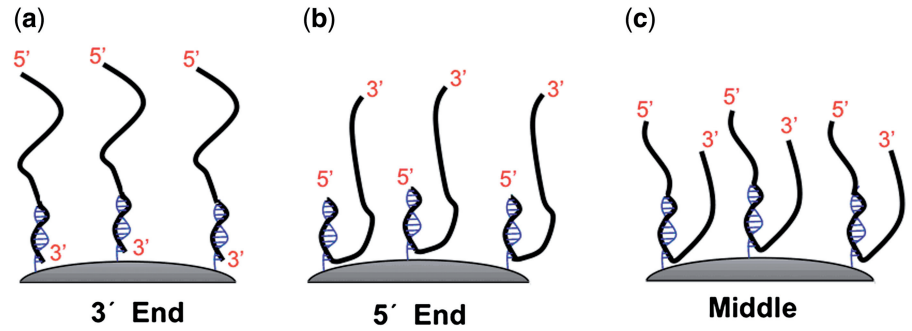

Scheme 3. Illustration of possible strand conformations for (**a**) **3′ End**, (**b**) **5′ End** and (**c**) **Middle** targets following successful hybridization events with immobilized **P15** strands.

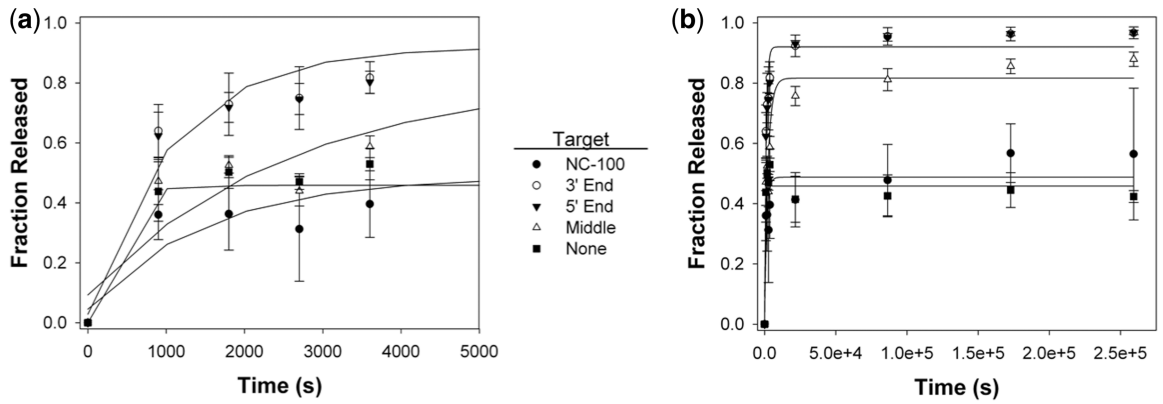

Figure 4. Fraction of reporter strands released from **P15:T11** dsProbes as a function of incubation time with various long targets after the first (**a**)1 h and (**b**)72 h.

but not negligible (42–56%). We attribute the similar release profiles of these two cases to the weak affinity of the **P15:T11** dsProbe allowing for some duplex dissociation over the long experimental timeframe. Though these controls show moderate release of the reporter strands from the dsProbes, significantly more reporter strand release (88–97%) is observed in the presence of targets containing the 15 base-long complementary recognition segment. For these long complementary targets, the overall trends in the release profiles are similar to those observed after incubation with the short 15 base-long target, though with some notable differences. As shown in Figure 4, for the **3′ End** and **5′ End** targets, a 6 h incubation time is required to release ~90% of the reporter strands from **P15:T11** dsProbes, whereas the same release is achieved in ~15 min by the short **T15** target in Figure 3. This difference indicates that the release kinetics are slowed by embedding the recognition segment within a longer model target system. Ultimately, fewer reporter strands are released from **P15:T11** dsProbes in the presence of the **Middle** target (~88%) than in the presence of the **3′ End** and **5′ End** targets (~97%). Thus, for this low affinity dsProbe, the location of the recognition sequence has a modest though observable effect on reporter strand release from the dsProbe. The close correlation in fraction released for samples incubated with **3′ End** and **5′ End** targets is somewhat surprising since the **3′ End** target case ideally has a more favorable orientation for allowing the unhybridized segment to extend away from the particle surface and other immobilized strands. Evidently, orientation of the **5′ End** target is either achieved with a similar readiness to the **3′ End** target or is inconsequential as the results for these two long targets correspond very closely to one another. The fraction released for the **Middle** target, on the other hand, is less than that of the **3′ End** and **5′ End** targets. Thus, the two non-hybridizing segments flanking the recognition element may impose an effectively greater electrosteric footprint than a single long thymine chain and obstruct the anti-parallel orientation necessary for duplexes to form. Though suppressed, reporter release does occur over time indicating that this obstruction slows, but does not prevent strand displacement events for long targets with the complementary segment embedded at various locations along the strand.

While substantial reporter strand loss is observed for these low affinity dsProbes in the absence of complementary target, reporter loss nearly doubles in the presence of complementary long targets. This disparity indicates that thermal dissociation alone is not responsible for the substantial reduction in the duplex density over time for these relatively weak dsProbes. In the presence of

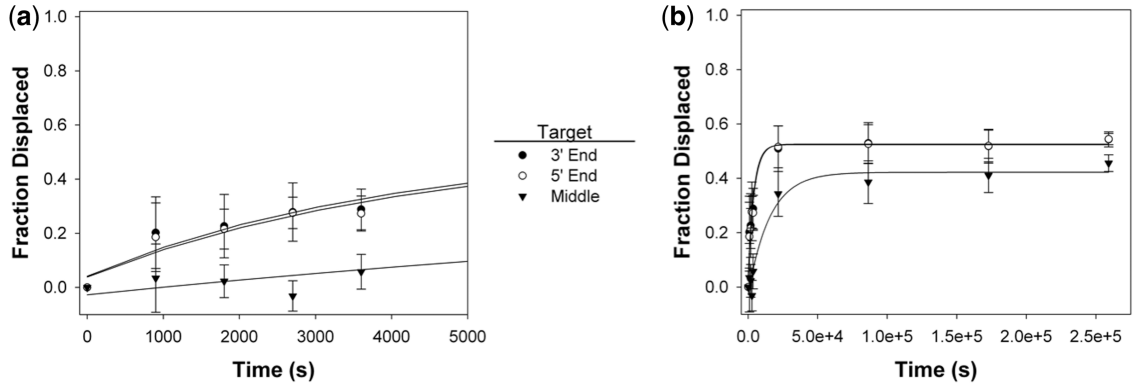

Figure 5. Fraction of reporter strands displaced from **P15:T11** dsProbes as a function of incubation time with various long complementary targets after the first (**a**)1 h and (**b**) 72 h.

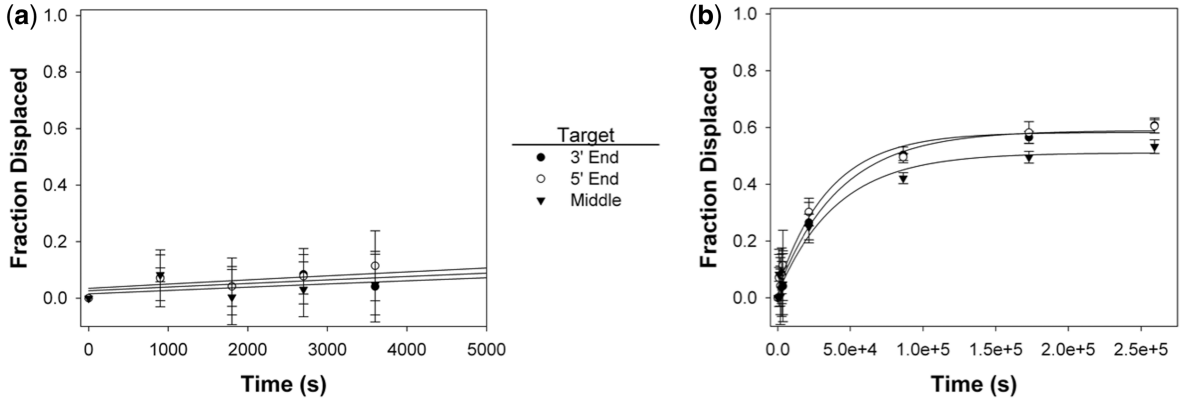

Figure 6. Fraction of reporter strands displaced from **P15:T15m** dsProbes as a function of incubation time with various long complementary targets after the first (**a**)1 h and (**b**) 72 h.

complementary targets, any additional loss of the reporter strands can be attributed to exchanging a significant portion of the shorter reporter strands for the longer complementary targets. To separate out the contribution of thermal dissociation, the fraction released in the absence of any target (**None**) was subtracted from the release profiles for each competitive target to generate displacement profiles. The resulting fraction *displaced* thus represents the reporter strand loss from dsProbes due to successful strand displacement by the target. Figure 5 shows the fraction of the reporter strands in **P15:T11** dsProbes displaced by various long targets. As expected, the overall trends observed in the displacement profiles shown in Figure 5 match the release profiles of Figure 4; however, the plateau values are lowered by ~40% in the displacement profiles for this low affinity dsProbe due to the significant contribution of thermal dissociation to reporter loss. The release profiles of another perfectly-matched duplex, the high affinity **P15:T13** dsProbe, were also studied following incubation with each of the long targets (Supplementary Figure S2). While dissociation effects are much less prominent, the release profiles for this high affinity dsProbe system do not approach an equilibrium plateau value within the experimental timeframe and thus were not evaluated further.

Figure 6 shows the strand displacement activity of the other low affinity dsProbe, **P15:T15m**, with each of the four model long targets examined. For the **P15:T15m** dsProbe, the time-dependent fraction of reporter strands displaced follows similar trends to that of the low affinity **P15:T11** dsProbe shown in Figure 5 though more time is required for the longer mismatched dsProbe to reach its plateau value. Once again, a greater fraction of reporter strands are displaced by the **3′ End** and **5′ End** targets than by the **Middle** target. In the absence of targets, comparison of the release profiles shown in supplementary data (Supplementary Figure S3) and Figure 4 indicates the **P15:T15m** dsProbe system (26% reporter loss) is less susceptible to thermal dissociation than **P15:T11** dsProbe system (42% reporter loss) despite their identical affinity rankings. The increased proclivity of **P15:T11** to allow reporter strands to even partially dissociate from the dsProbes may also give rise to its faster displacement behavior. In order to further elucidate the differences in strand displacement behavior between the various long targets for two dsProbe systems with identical affinity rankings, observed displacement rates were determined for both the low affinity **P15:T11** and **P15:T15m** dsProbe systems.

Table 3. Observed displacement rates, k_{obs} (s^{-1}) for **P15:T11** and **P15:T15m** dsProbe systems in the presence of various long targets possessing a 15 base-long, embedded recognition segment complementary to the immobilized **P15** sequence

Target nomenclature	k_{obs} (s^{-1})	
	P15:T11 dsProbe	P15:T15m dsProbe
3′ End	2.0×10^{-4}	2.3×10^{-5}
5′ End	2.0×10^{-4}	2.8×10^{-5}
Middle	6.4×10^{-5}	2.4×10^{-5}

Determining an observed displacement rate

To quantify the kinetics of strand displacement events, an observed displacement rate, k_{obs}, was analytically determined as described in detail in the experimental methods section. Briefly, the reported k_{obs} values correspond to pairs of dsProbe–target systems that both (i) reach or nearly reach an equilibrium plateau in the displacement profiles within the 72 h experimental timeframe and (ii) have $R^2 > 0.9$. These two conditions were only met by the two low affinity **P15:T11** and **P15:T15m** dsProbes systems shown in Figure 5 and Figure 6, but not by the high affinity **P15:T13** dsProbe (Supplementary Figure S2). Table 3 shows the resulting k_{obs} values for these two low affinity dsProbes with various long targets. Notably, the estimated diffusion-based collision rate between the microspheres and target strands is $\sim 10^6 s^{-1}$ and thus diffusion events do not serve as the rate-limiting step for secondary duplex formation. The differences in k_{obs} values for **P15:T11** further confirm the faster displacement activity by the two end targets ($10^{-4} s^{-1}$) compared to the **Middle** target ($10^{-5} s^{-1}$). In general, these observed displacement rate values are faster than the values ($\sim 10^{-6} s^{-1}$) reported by Reynaldo *et al.* (47) for soluble (i.e. not immobilized) duplexes at relatively low temperatures (30°C). In Reynaldo's work, displacement involved a competitive or secondary target that was identical in sequence and length as the initial hybridization partner. Consequently, their system does not involve sequence-based affinity differences to specifically favor competitive displacement. The overall faster displacement rates in the current study are, therefore, not surprising as the dsProbes formed with the reporter strands are intentionally designed to have lower affinity than the secondary duplexes formed with the target strands. Moreover, successful competitive hybridization occurs for all three 100 base-long targets studied and indicates that the location alone of the complementary sequence segment in the target does not ultimately inhibit hybridization events with the immobilized dsProbes. This conclusion holds promise for future studies with colloid-based detection platforms investigating an array of long sequences of varying base compositions in which other effects such as intrastrand self-loops on duplex formation are the central focus.

DISCUSSION

In the current study, dsProbes immobilized on microspheres were employed to interrogate long targets with an embedded recognition segment. As most physiologically relevant nucleic acid targets do not exist as short segments of nucleic acids, the ability to efficiently interrogate recognition motifs within longer strand contexts is necessary for effective detection platforms. Thus, one of the goals of the current study was to assess the kinetics of reporter strand displacement by a long target with a short recognition segment embedded at various locations. In order to better understand how sequence design of the dsProbe affects competitive displacement of reporter strands by various targets, affinity differences between the labeled reporter strand and the target of interest were incorporated by selectively including sequence mismatches in dsProbes of varying duplex length. The inclusion of a center mismatch alone has a profound effect on the affinity ranking of a given dsProbe. All dsProbes with a center mismatch are classified as either low or lowest affinity dsProbes while most of the perfectly complementary analogs are high affinity dsProbes. Displacement activity of the reporter strands from the dsProbes is also strongly affected by the presence of a center mismatch. For example, insertion of a center mismatch transforms a largely non-responsive dsProbe, **P15:T15**, into the responsive **P15:T15m** dsProbe.

The second sequence design strategy considered in this study was the inclusion of small variations in the base length of the duplex segment of the dsProbe. For the relatively short dsProbes studied here, these small differences in the duplex length have a significant effect on both dsProbe affinity and the resulting strand displacement activity by long targets. **P15:T11**, a low affinity dsProbe, has a low initial duplex density and exhibits a significant loss of reporter strands due to thermal dissociation in the absence of targets. With only two additional bases in the duplex segment, the **P15:T13** dsProbes, on the other hand, exhibit limited thermal dissociation. Additionally, small differences in the number of intentionally unoccupied bases next to the original duplex results in the distinct profiles for these two dsProbes in the presence of complementary targets. The reporter strands of **P15:T11** are quickly displaced while those of **P15:T13** undergo only limited release. The availability of four unhybridized bases in the **P15:T11** dsProbe may serve as an effective toehold for the secondary duplexes to first nucleate in the presence of the original hybridization partner and then, displace the shorter partner strand as hybridization progresses. While the toehold length appears to affect strand displacement, it is likely that the response differences of **P15:T11** and **P15:T13** dsProbes arise from a combination of affinity differences and base length in the toehold regions. The work of Li *et al.* (30) has also reported faster displacement rates for soluble (i.e. not immobilized) dsProbes as their respective toehold lengths (up to 7 bases) increase.

The dsProbes that contain both a toehold and center mismatch, namely **P15:T11m** and **P15:T13m**, are ranked as the lowest affinity dsProbe and a low affinity dsProbe, respectively. Incubation with the **T15** target strand results in the loss of nearly all reporter strands within just the first hour. Though seemingly responsive as dsProbes, the weak stability of **P15:T11m** does not make them ideal

candidates for target detection. Combined, these results demonstrate that the central challenge of a competition-based detection platform is the successful design of dsProbes with sufficient affinity to remain stable over time while still efficiently responding to the presence of particular targets. As seen from our results, the current system requires a significant reaction time in order for displacement to reach a plateau value with these long targets. Delays in reaching equilibrium can be attributed to the larger electrosteric repulsion associated with the 100 base-long targets compared to the 15 base-long reporter strands. In fact, in a separate study involving 20 base-long immobilized probes and perfectly complementary targets ranging 8–16 bases in length, we reported that the 16 base-long targets actually formed *fewer* duplexes than the 14 base-long targets (40). Given the fact that its higher affinity should drive more duplex formation for 16 base-long targets, we concluded that even small base length extensions can result in sufficient electrosteric repulsions and possible substrate interference that hinder otherwise more favorable duplex formation conditions. Thus, in the current system involving much longer target strands (but with comparable 15 base-long duplex-forming segments), the relatively long, unhybridized segments associated with the secondary duplexes are even more likely to delay neighboring reporter:probe duplexes from undergoing displacement events. In ongoing work, we are testing different strategies to promote more efficient displacement events by widening the lateral spacing between dsProbes as well as altering the dsProbe presentation by reorienting the toehold region (of unhybridized bases) *away* from the microsphere surface to better facilitate target strand hybridization.

CONCLUSIONS

The current research considers the influence of target strand context on the displacement of reporter strands from immobilized dsProbes. By varying the base length and fidelity in the immobilized dsProbes, these studies specifically aim to improve our fundamental understanding of the time-dependent strand displacement behavior of targets in which the complementary segment itself is embedded within a longer DNA strand. Here, kinetics studies were conducted under isothermal, room temperature conditions to monitor successful reporter strand displacement events by unlabeled targets. Importantly, the responsiveness of the dsProbes depended on the intrinsic affinity of the dsProbe tuned through readily accessible sequence design strategies such as incorporating a short single-stranded toehold region or a mismatch within the dsProbe duplex. Collectively, our results illustrate that the dual challenge to successful reporting of target hybridization events involves optimizing the sequence design to maximize dsProbe formation and stability in the absence of a target of interest while promoting the ready responsiveness of dsProbes to the presence of a complementary target. While the choice of dsProbe sequences was found to play a pivotal role, the location itself of the complementary sequence segment in the 100 base-long targets does not ultimately inhibit hybridization events or even have a pronounced effect on the kinetics or extent of reporter strand displacement from dsProbes. The success of competitive displacement events between all long targets and relatively short immobilized dsProbes in the current study thus holds promise for employing colloidal particles for a variety of nucleic acid-based reaction schemes, particularly if the timing for displacement events can be accelerated. To this end, we are currently exploring the effect of re-orienting the toehold region away from the microsphere surface towards the free dangling end of the dsProbe. Similarly, we are examining the ability of our particle-based dsProbes to discriminate between nearly identical oligonucleotide targets.

SUPPLEMENTARY DATA

Supplementary Data are available at NAR Online.

ACKNOWLEDGEMENTS

The authors thank Dr Phil Santangelo for his helpful and insightful review of the manuscript as well as Chris Tison and James Hardin for helpful discussions. Additionally, the authors thank Johnafel Crowe for his guidance with flow cytometry measurements.

FUNDING

The Georgia Cancer Coalition Distinguished Scholar program; the Army Research Office (W911NF-09-1-0479); the Georgia Institute of Technology; Funding for open access charge: Army Research Office.

Conflict of interest statement. None declared

REFERENCES

1. Calladine,C.R., Drew,H.R., Luisi,B.F. and Travers,A.A. (2004) *Understanding DNA*, 3rd edn. Elsevier Academic Press, Amsterdam, pp. 18–38.
2. Lipshutz,R.J., Fodor,S.P.A., Gingeras,T.R. and Lockhart,D.J. (1999) High density synthetic oligonucleotide arrays. *Nat. Genet.*, **21**, 20–24.
3. Halperin,A., Buhot,A. and Zhulina,E.B. (2006) Hybridization at a surface: the role of spacers in DNA microarrays. *Langmuir*, **22**, 11290 – 11304.
4. Call,D.R., Borucki,M.K. and Loge,F.J. (2003) Detection of bacterial pathogens in environmental samples using DNA microarrays. *J. Microbiol. Methods*, **53**, 235–243.
5. Pease,A.C., Solas,D., Sullivan,E.J., Cronin,M.T., Holmes,C.P. and Fodor,S.P.A. (1994) Light-generated oligonucleotide arrays for rapid DNA sequence analysis. *Proc. Natl Acad. Sci. USA*, **91**, 5022–5026.
6. Schena,M., Shalon,D., Davis,R.W. and Brown,P.O. (1995) Quantitative monitoring of gene expression patterns with a complementary DNA microarray. *Science*, **270**, 467–470.
7. Hacia,J.G., Brody,L.C., Chee,M.S., Fodor,S.P.A. and Collins,F.S. (1996) Detection of heterozygous mutations in BRCA1 using high density oligonucleotide arrays and two-color fluorescence analysis. *Nat. Genet.*, **14**, 441–447.
8. Ramsay,G. (1998) DNA chips: State-of-the art. *Nat. Biotechnol.*, **16**, 40–44.

9. Dunbar,S.A., Zee,C.A.V., Oliver,K.G., Karem,K.L. and Jacobson,J.W. (2003) Quantitative, multiplexed detection of bacterial pathogens: DNA and protein applications of the Luminex LabMAP^{TM} system. *J. Microbiol. Methods*, **53**, 245–252.
10. Lu,J., Getz,G., Miska,E.A., Alvarez-Saavedra,E., Lamb,J., Peck,D., Sweet-Cordero,A., Ebert,B.L., Mak,R.H., Ferrando,A.A. *et al.* (2005) MicroRNA expression profiles classify human cancers. *Nature*, **435**, 834–838.
11. Stevens,P.W., Henry,M.R. and Kelso,D.M. (1999) DNA hybridization on microparticles: determining capture-probe density and equilibrium dissociation constants. *Nucleic Acids Res.*, **27**, 1719–1727.
12. Chen,C., Wang,W., Ge,J. and Zhao,X.S. (2009) Kinetics and thermodynamics of DNA hybridization on gold nanoparticles. *Nucleic Acids Res.*, **37**, 3756–3765.
13. Dunbar,S. and Jacobsen,J.W. (2007) Quantitative, multiplexed detection of Salmonella and other pathogens by Luminex^{R} xMAP^{TM} suspension arrays. In Schatten,H. and Eisenstark,A. (eds), *Salmonella: Methods and Protocols*. Humana Press, Inc., Totowa, pp. 1–19.
14. Baldi,P. and Hatfield,G.W. (2002) *DNA Microarrays and Gene Expression: From Experiments to Data Analysis and Modeling*. Cambridge University Press, London.
15. Knudsen,S. (2004) *Guide to Analysis of DNA Microarray Data*, 2nd edn. John Wiley & Sons, Inc., NY.
16. Fish,D.J., Horne,M.T., Brewood,G.P., Goodarzi,J.P., Alemayehu,S., Bhandiwad,A., Searles,R.P. and Benight,A.S. (2007) DNA multiplex hybridization on microarrays and thermodynamic stability in solution: a direct comparison. *Nucleic Acids Res.*, **35**, 7197–7208.
17. Urakawa,H., Fantroussi,S.E., Smidt,H., Smoot,J.C., Tribou,E.H., Kelly,J.J., Noble,P.A. and Stahl,D.A. (2003) Optimization of single-base-pair mismatch discrimination in oligonucleotide microarrays. *Appl. Environ. Microbiol.*, **69**, 2848–2856.
18. Dai,H., Meyer,M., Stepaniants,S., Ziman,M. and Stoughton,R. (2002) Use of hybridization kinetics for differentiating specific from non-specific binding to oligonucleotide microarrays. *Nucleic Acids Res.*, **30**, e86.
19. Okahata,Y., Kawase,M., Niikura,K., Ohtake,F., Furusawa,H. and Ebara,Y. (1998) Kinetic measurements of DNA hybridization on an oligonucleotide-immobilized 27-MHz quartz crystal microbalance. *Anal. Chem.*, **70**, 1288–1296.
20. Peterson,A.W., Heaton,R.J. and Georgiadis,R.M. (2001) The effect of surface probe density on DNA hybridization. *Nucleic Acids Res.*, **29**, 5163–5168.
21. Peterson,A.W., Wolf,L.K. and Georgiadis,R.M. (2002) Hybridization of mismatched or partially matched DNA at surfaces. *J. Am. Chem. Soc.*, **124**, 14601–14607.
22. Tawa,K., Yao,D. and Knoll,W. (2005) Matching base-pair number dependence of the kinetics of DNA-DNA hybridization studied by surface plasmon fluorescence spectroscopy. *Biosens. Bioelectron.*, **21**, 322–329.
23. Glazer,M., Fidanza,J.A., McGall,G.H., Trulson,M.O., Forman,J.E., Suseno,A. and Frank,C.W. (2006) Kinetics of oligonucleotide hybridization to photolithographically patterned DNA arrays. *Anal. Biochem.*, **358**, 225–238.
24. Green,C. and Tibbetts,C. (1981) Reassociation rate limited displacement of DNA strands by branch migration. *Nucleic Acids Res.*, **9**, 1905–1918.
25. Vary,C.P.H. (1987) A homogeneous nucleic acid hybridization assay based on strand displacement. *Nucleic Acids Res.*, **15**, 6883–6897.
26. Vary,C.P.H., McMahon,F.J., Barbone,F.P. and Diamond,S.E. (1986) Nonisotopic detection methods for strand displacement assays of nucleic acids. *Clin. Chem.*, **32**, 1696–1701.
27. Ellwood,M.S., Collins,M., Fritsch,E.F., Williams,J.I., Diamond,S.E. and Brewen,J.G. (1986) Strand displacement applied to assays with nucleic acid probes. *Clin. Chem.*, **32**, 1631–1636.
28. Wolf,S.F., Haines,L., Fisch,J., Kremsky,J.N., Dougherty,J.P. and Jacobs,K. (1987) Rapid hybridization kinetics of DNA attached to submicron latex particles. *Nucleic Acids Res.*, **15**, 2911–2926.
29. Homann,M., Nedbal,W. and Sczakiel,G. (1996) Dissociation of long-chain duplex RNA can occur via strand displacement *in vitro*: biological implications. *Nucleic Acids Res.*, **24**, 4395–4400.
30. Li,Q., Luan,G., Guo,Q. and Liang,J. (2002) A new class of homogeneous nucleic acid probes based on specific displacement hybridization. *Nucleic Acids Res.*, **30**, e5.
31. Tierney,S. and Stokke,B.T. (2009) Development of an oligonucleotide functionalized hydrogel integrated on a high resolution interferometric readout platform as a label-free macromolecule sensing device. *Biomacromolecules*, **10**, 1619–1626.
32. Kim,W.J., Sato,Y., Akaike,T. and Maruyama,A. (2003) Cationic comb-type copolymers for DNA analysis. *Nat. Mater.*, **2**, 815–820.
33. Seferos,D.S., Giljohann,D.A., Hill,H.D., Prigodich,A.E. and Mirkin,C.A. (2007) Nano-flares: Probes for transfection and mRNA detection in living cells. *J. Am. Chem. Soc.*, **129**, 15477–15479.
34. Yang,S.Y., Son,S., Jang,S., Kim,H., Jeon,G., Kim,W.J. and Kim,J.K. (2011) DNA-functionalized nanochannels for SNP detection. *Nano Lett.*, **11**, 1032–1035.
35. Yurke,B., Tuberfield,A.J., Mills,A.P.J., Simmel,F.C. and Neumann,J.L. (2000) A DNA-fuelled molecular machine made of DNA. *Nature*, **406**, 605–608.
36. Simmel,F.C. and Yurke,B. (2001) Using DNA to construct and power a nanoactuator. *Phys. Rev. E*, **63**, 041913.
37. Tuberfield,A.J., Mitchell,J.C., Yurke,B., Mills,A.P.J., Blakey,M.I. and Simmel,F.C. (2003) DNA fuel for free-running nanomachines. *Phys. Rev. Lett.*, **90**, 118102.
38. Liu,C., Jonoska,N. and Seeman,N.C. (2009) Reciprocal DNA nanomechanical devices controlled by the same set strands. *Nano Lett.*, **9**, 2641–2647.
39. Yan,H., Zhang,X., Shen,Z. and Seeman,N.C. (2002) A robust DNA mechanical device controlled by hybridization topology. *Nature*, **415**, 62–65.
40. Tison,C.K. and Milam,V.T. (2007) Reversing DNA-mediated adhesion at a fixed temperature. *Langmuir*, **23**, 9728–9736.
41. Baker,B.A. and Milam,V.T. (2010) DNA density-dependent assembly behavior of colloidal micelles. *Langmuir*, **26**, 9818–9826.
42. Tison,C.K. and Milam,V.T. (2010) Programming the kinetics and extent of colloidal disassembly using a DNA trigger. *Soft Matter*, **6**, 4446–4453.
43. Hazarika,P., Ceyhan,B. and Niemeyer,C.M. (2004) Reversible switching of DNA-gold nanoparticle aggregation. *Angew. Chem. Int. Ed.*, **43**, 6469–6471.
44. Sebba,D.S., Mock,J.J., Smith,D.R., LaBean,T.H. and Lazarides,A.A. (2008) Reconfigurable core-satellite nanoassemblies as molecularly-driven plasmonic switches. *Nano Lett.*, **8**, 1803–1808.
45. Maye,M.M., Kumara,M.T., Nykypanchuk,D., Sherman,W.B. and Gang,O. (2009) Switching binary states of nanoparticle superlattices and dimer clusters by DNA strands. *Nat. Nanotechnol.*, **5**, 116–120.
46. Porschke,D. and Eigen,M. (1971) Co-operative non-enzymic base recognition III. Kinetics of the helix-coil transition of the oligoribouridylic oligoriboadenylic acid system and of oligoriboadenylic acid alone at acidic pH. *J. Mol. Biol.*, **62**, 361–381.
47. Reynaldo,L.P., Vologodskii,A.V., Neri,B.P. and Lyamichev,V.I. (2000) The kinetics of oligonucleotide replacements. *J. Mol. Biol.*, **297**, 511–520.
48. Zhang,D.Y. and Winfree,E. (2009) Control of DNA strand displacement kinetics using toehold exchange. *J. Am. Chem. Soc.*, **131**, 17303–17314.
49. Genot,A.J., Zhang,D.Y., Bath,J. and Tuberfield,A.J. (2011) Remote toehold: a mechanism for flexible control of DNA hybridization kinetics. *J. Am. Chem. Soc.*, **133**, 2177–2182.
50. Dunbar,S.A. (2006) Applications of Luminex^{R} xMAP^{TM} technology for rapid, high-throughput multiplexed nucleic acid detection. *Clin. Chim. Acta*, **363**, 71–82.
51. Santangelo,P.J., Nix,B., Tsourkas,A. and Bao,G. (2004) Dual FRET molecular beacons for mRNA detection in living cells. *Nucleic Acids Res.*, **32**, e57.
52. Lubin,A.A., Hunt,B.V.S., White,R.J. and Plaxco,K.W. (2009) Effects of probe length, probe geometry, and redox-tag placement

on the performance of the electrochemical E-DNA sensor. *Anal. Chem.*, **81**, 2150–2158.
53. Cram,L.S. (2002) Flow cytometry, an overview. *Methods Cell Sci.*, **24**, 1–9.
54. Fulton,R.J., McDade,R.L., Smith,P.L., Kienker,L.J. and Kettman,J.R. Jr (1997) Advanced multiplexed analysis with the FlowMetrix^{TM} system. *Clin. Chem.*, **43**, 1749–1756.
55. Battersby,B.J. and Trau,M. (2002) Novel miniaturized systems in high-throughput screening. *Trends Biotechnol.*, **20**, 167–173.
56. Markham,N.R. and Zuker,M. *MFold*, , http://dinamelt.bioinfo.rpi.edu/hybrid2.php. (16 September 2008, date last accessed).
57. Markham,N.R. and Zuker,M. (2005) DINAMelt web server for nucleic acid melting prediction. *Nucleic Acids Res.*, **33**, W577–W581.
58. Markham,N.R. and Zuker,M. (2008) UNAFold: software for nucleic acid folding and hybriziation. In Keith,J.M. (ed.), *Bioinformatics, Volume II. Structure, Functions and Applications*. Humana Press, Totowa, pp. 3–31.
59. Zhang,Y., Hammer,D.A. and Graves,D.J. (2005) Competitive hybridization kinetics reveals unexpected behavior patterns. *Biophys. J.*, **89**, 2950–2959.